Advanced Composite Materials
Publication details, including instructions for authors and subscription information:
http://www.tandfonline.com/loi/tacm20

Characterization of mechanical properties and bioactivity of hydroxyapatite/β-tricalcium phosphate composites

Satoshi Kobayashi[a] & Takuma Murakoshi[a]
[a] Department of Mechanical Engineering, Tokyo Metropolitan University, 1-1 Minami-Osawa, Hachioji, Tokyo, 192-0397, Japan.
Published online: 09 Oct 2013.

To cite this article: Satoshi Kobayashi & Takuma Murakoshi (2014) Characterization of mechanical properties and bioactivity of hydroxyapatite/β-tricalcium phosphate composites, Advanced Composite Materials, 23:2, 163-177, DOI: 10.1080/09243046.2013.844897

To link to this article: http://dx.doi.org/10.1080/09243046.2013.844897

Advanced Composite Materials, 2014
Vol. 23, No. 2, 163–177, http://dx.doi.org/10.1080/09243046.2013.844897

Characterization of mechanical properties and bioactivity of hydroxyapatite/β-tricalcium phosphate composites

Satoshi Kobayashi* and Takuma Murakoshi

Department of Mechanical Engineering, Tokyo Metropolitan University, 1-1 Minami-Osawa, Hachioji, Tokyo 192-0397, Japan

(*Received 27 March 2013; accepted 31 May 2013*)

Bioactive ceramics attracts much attention as materials for bone implants, because of their high biocompatibility. For example, hydroxyapatite (HA) has bone-bonding ability through a bone-like apatite layer in body environment and β-tricalcium phosphate (β-TCP) has a high bioresorbability in body environment. In this study, HA/β-TCP composites with different β-TCP content (0, 10, 20, and 30 wt.%) were prepared by wet mixing of HA and β-TCP powders, compaction of the powder mixture and sintering. Bending strength of HA/β-TCP composites was measured before and after soaking in simulated body fluid (SBF). The bioactivity of HA/β-TCP composites was also evaluated by soaking in SBF. To improve mechanical properties of HA/β-TCP composites, effects of additive of SiO_2 and MgO were also investigated. It was found that the several mechanical properties and ability of apatite formation decreased with β-TCP content. It was also found that the change in bending strength after soaking depended on its surface reaction in SBF and porosity. Addition of SiO_2 did not improve mechanical properties and bioactivity. On the other hand, additive of MgO improved several mechanical properties, but lowered the bioactivity in SBF.

Keywords: hydroxyapatite; β-tricalcium phosphate; mechanical property; simulated body fluid

1. Introduction

Bioactive ceramics attracts attentions as materials of bone implants, because of their high biocompatibility. Among them, hydroxyapatite ($Ca_{10}(PO_4)_6(OH)_2$: HA) has bone-bonding ability through a bone-like apatite layer which is formed on its surface in body environment. On the other hand, β-tricalcium phosphate ($Ca_3(PO_4)_2$: β-TCP) has high bioresorbability in body environment. In previous investigation, mechanical properties of HA and β-TCP [1–3] were reported. These bioactive ceramics have no necessity of re-operation after complete curing because of their high biocompatibility. It seems that HA/β-TCP composites could have good functions of both HA and β-TCP. For HA/β-TCP composites, the ratio between HA and β-TCP is a very important parameter to determine the rate of apatite formation and bioresorbability in body environment. From this point of view, mechanical properties of HA/β-TCP composites which were prepared by partial decomposition from HA into β-TCP during sintering were

*Corresponding author. Email: koba@tmu.ac.jp

investigated.[4,5] In this method, however, it is difficult to control the ratio of the partial decomposition from HA into β-TCP. On the other hand, the ratio of HA/β-TCP is easily controlled by sintering of HA and β-TCP powder mixture. Since it is difficult to obtain dense composites by sintering of different kind of powder, little study about HA/β-TCP composites prepared by powder mixture has been investigated in terms of its mechanical properties and bioactivity in body environment. Therefore, in order to improve sinterability, sintering additives have been discussed. Ryu et al. [6] investigated effects of MgO as a sintering additive for a HA/β-TCP composite with weight ratio of 50/50. For a tailor-made treatment considering a location and degree of a disease HA/β-TCP composite, it is important to clarify effects of HA/β-TCP ratio on mechanical properties and bone-formation ability of HA/β-TCP. Despite the importance, little study about the effect of HA/β-TCP ratio on mechanical properties and bioactivity has been investigated.

This study attempts to evaluate mechanical properties and bioactivity of HA/β-TCP composites which are prepared by sintering of HA and β-TCP powder mixture. To improve mechanical properties of HA/β-TCP composites, effects of additive of SiO_2 and MgO were also investigated, because MgO is reported in other literature [6] and SiO_2 is one of the component materials of bioglass.[7]

2. Experimental procedures

2.1. Preparation of specimen

Measured amount of HA powder (Taihei Chemical Industrial Co. Ltd., Japan, HAP-200) and β-TCP powder (Taihei Chemical Industrial Co. Ltd., Japan, β-TCP-100) were dispersed in ethanol with β-TCP content of 0, 10, 20, and 30 wt.%. After stirring for 24 h, ethanol was evaporated from slurry to obtained HA/β-TCP powder mixture. The resultant powder was then uniaxially pressed in a die at 100 MPa. The green compact was sintered in a furnace. The sintering employed a holding time of 5 h at 1250 °C with heating rate of 10 °C/min, and cooling in the furnace for 5 h to the room temperature. The sintering compact was grinded, polished, and cut into rectangular specimens of 18 mm × 2.0 mm × 1.5 mm. The tensile surface in bending test as mentioned below was polished. Finally, the corners of specimen were chamfered by an emery paper.

In order to investigate effects of additive, 1 wt.% of SiO_2 powder or MgO powder (Wako Pure Chemical Industries Co. Ltd., Japan) was added in ethanol when HA/β-TCP was stirred, only for β-TCP content of 30 wt.%. The schematic illustration of process of specimen fabrication is shown in Figure 1.

2.2. Relative density measurement

Relative density was measured by Archimedes method, according to JIS R 1634. First, the weight of specimen (W_1: dry weight) was measured, then the specimen was boiled for over 3 h and cooled to the room temperature. After that, the weight of the specimen in the water (W_2: weight in water) was measured. Next, the specimen was removed from the water, and then the water on the specimen was removed using paper. After that, the weight (W_3: water-saturated weight) was measured. Relative density was calculated from the following equations,

$$\rho_b = \frac{W_1}{W_3 - W_2} \times \rho_1, \quad \rho_r = \frac{\rho_b}{\rho_2} \times 100 \tag{1}$$

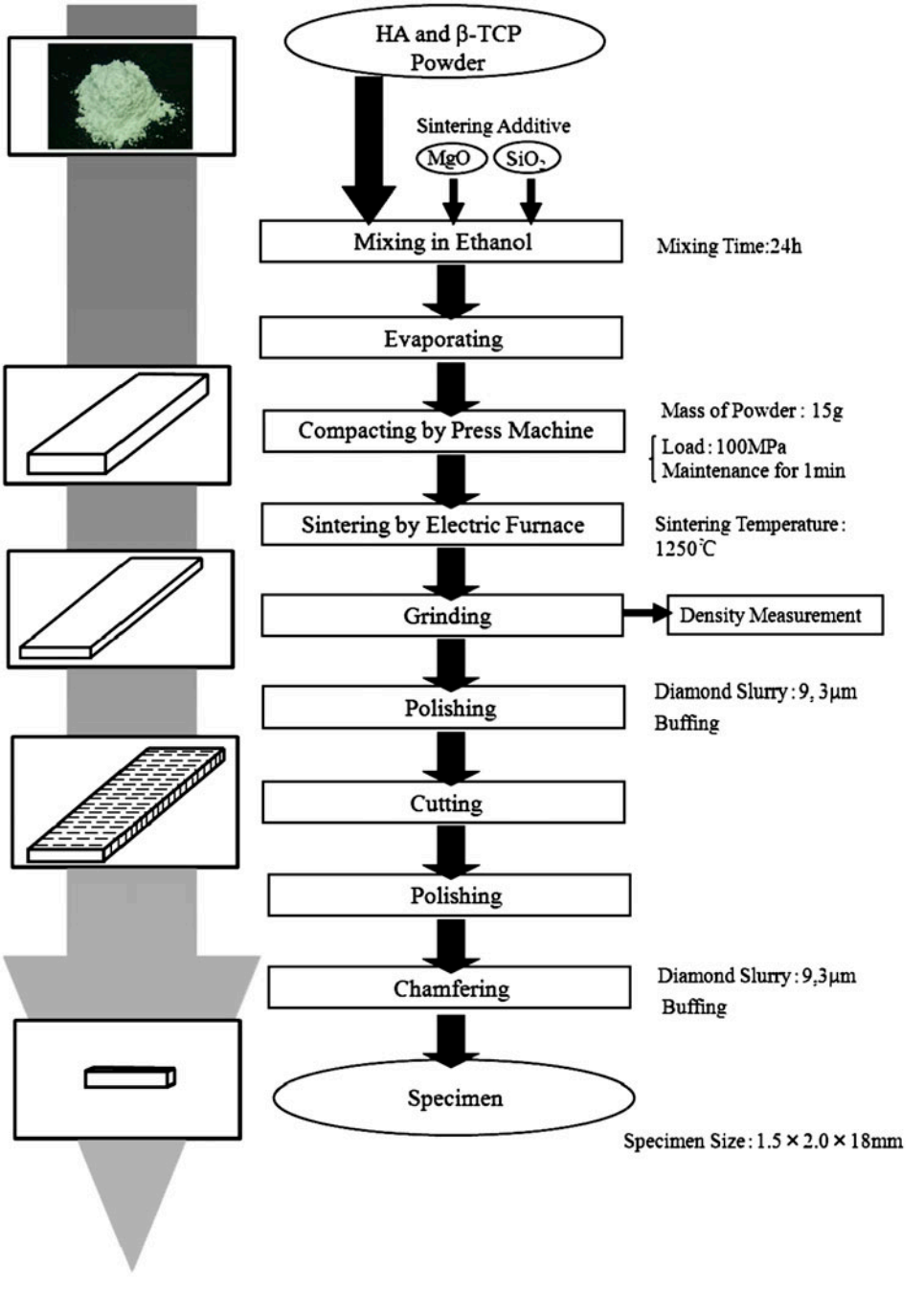

Figure 1. Process of specimen fabrication.

where ρ_b is the bulk density [g/cm^3], W_1 is the dry weight [g], W_2 is weight in water [g], W_3 is the water-saturated weight [g], ρ_1 is the density of water [g/cm^3], ρ_r is the relative density [%], and ρ_2 is the theoretical density of powder [g/cm^3].

2.3. Grain size measurement

Average grain size of the sample was measured as following steps. First, thermal etching was applied by using a furnace. The program was employed with a holding time of 1 h at 1150 °C, with heating rate of 50 °C/min, and furnace cooling to the room temperature. Then, average grain size was measured by line intercept method using the picture observed by scanning electron microscopy (SEM), as shown in Figure 2. Average grain size was calculated from the following equations,

$$A = \frac{d_1 d_2}{n_1 n_2 M^2}, \qquad d = \sqrt{\frac{4A}{\pi}} \tag{2}$$

where A is the average grain area [mm^2], d_1 is the horizontal line length [mm], d_2 is the vertical line length [mm], M is the magnification of picture, n_1 is the number of horizontal grain, n_2 is the number of vertical grain, and d is the average grain size [mm].

2.4. X-ray diffraction measurement

To evaluate the phase composition, X-ray powder diffraction measurement (XRD) was performed on an XRD (Rigaku, RINT-TTRIII, Japan), which had an X-ray source of Cu-Kα of 40 keV and 300 mA. The setting of XRD is shown in Table 1. Phase identification was done with the use of the software MDIJADE7.

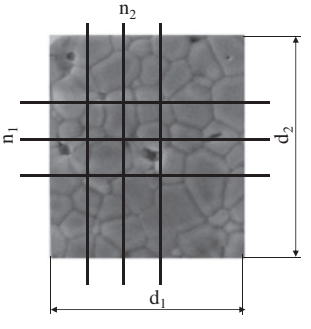

Figure 2. Line intercept method.

Table 1. Setting of XRD.

Scan method	Continuous scan method
Scan axis	$2\theta/\theta$
Measuring range	20–40 °
Sampling interval	0.05 °
Scan rate	1.00 °/min
Measurment method	Usual method
Tube voltage	40 keV
Tube current	300 mA
Divergence slit	2/3 °
Scattering slit	2/3 °
Receiver slit	0.30 mm

2.5. Four-point bending test

To evaluate the mechanical properties, four-point bending tests were performed with a cross-head speed of 0.1 mm/min with an universal testing machine (Shimadzu, AG-IS 50kN). The upper span was 5 mm, the lower span was 15 mm. Bending strength was calculated from the following equation,

$$\sigma_{\mathrm{B}} = \frac{3Fl}{bh^2} \tag{3}$$

where σ_{B} is the bending strength [MPa], F is the maximum applied load [N], l is the upper span [mm], h is the thickness [mm], and b is the width [mm].

2.6. Fracture toughness test

To measure Vickers hardness and fracture toughness and elastic coefficient, indentation fracture toughness test was performed with a microhardness testing machine (Shimadzu, Japan, DUH-211). Fracture toughness was calculated from the following equation,

$$K_{\mathrm{IC}} = 0.018\left(\frac{E}{HV}\right)^{\frac{1}{2}}\left(\frac{P}{c^{\frac{3}{2}}}\right) = 0.026\,\frac{E^{\frac{1}{2}}P^{\frac{1}{2}}a}{c^{\frac{3}{2}}} \tag{4}$$

where K_{IC} is the fracture toughness [Pa $\cdot$ $\mathrm{m}^{1/2}$], E is the elastic coefficient [Pa], HV is the Vickers hardness [Pa], P is the load [N], c is the half length of surface crack [m], and a is the half diagonal of Vickers indent [m].

2.7. Bioactivity

Simulated body fluid (SBF) was prepared to evaluate the behavior in body environment. SBF was proposed by Kokubo et al. to evaluate the *in vitro* bioactivity.[8] The ion concentrations of SBF used in this study are compared with the human blood plasma in Table 2. SBF was prepared by dissolving the reagent grade chemicals shown in Table 3 into distilled water and buffered with Tris and HCl to pH 7.4 at 37 °C. It is nearly equal to those in human blood plasma. The specimens were soaked in SBF at 37 °C up to four weeks. After soaking, bending strength was measured and the surface of specimens was examined by SEM to confirm the bone-like apatite formation.

Table 2. Ion concentration of SBF and human blood plasma.

Ion	SBF [mM/l]	Blood plasma [mM/l]
Na^+	142	142
K^+	5	5
Ca^{2+}	2.5	2.5
Mg^{2+}	1.5	1.5
Cl^-	18	104
HCO^{3-}	4.2	27
HPO_4^{2-}	1	1
SO_4^{2-}	0.5	0.5
Tris(hydroxymethyl)	100	–

Table 3. SBF composition.

Reagent	Mass
$CaCl_2 \cdot 2H_2O$	0.3676 g
$MgCl_2 \cdot 6H_2O$	0.3048 g
Na_2SO_4	0.0710 g
K_2HPO_4	0.1742 g
$NaHCO_3$	0.3528 g
KCl	0.2237 g
NaCl	7.9950 g
Tris	6.0568 g
HCl	4.5 ml (pH = 7.4)

3. Results and discussion

3.1. HA/β-TCP composites

3.1.1. Mechanical properties in the atmosphere

Figure 3 shows relative density of HA/β-TCP composites. Relative density of HA/β-TCP composites decreased with increasing β-TCP content. It is suggested that porosity increased with β-TCP content. Particularly in case of 30 wt.%, the relative density decreased significantly. This result suggests the poor sinterability of HA/β-TCP powder mixture.

Figure 4 shows SEM photographs of grain size of HA/β-TCP composites and grain size of HA/β-TCP composites calculated by Equation (2). Grain size of HA/β-TCP composites increased with β-TCP addition. SEM photographs in Figure 4 also show that samples of containing β-TCP had bimodal structure of grain distribution: larger grains and smaller grains. That is, abnormal grain growth occurred. It is speculated that β-TCP accelerated grain growth in HA/β-TCP composites.

Figure 5 shows bending strength of HA/β-TCP composites. It is found that bending strength of HA/β-TCP composites decreased by ~20% comparing with pure HA. This is because HA/β-TCP composites have more lower relative density, i.e. higher porosity, than pure HA. This is also because HA/β-TCP composites have larger grain size than pure HA.

Figure 6 shows SEM photographs of the fracture surface of HA/β-TCP composites. In each sample, it is found that transgranular fracture occurred. It can be seen from SEM photograph of fracture surface of 30 wt.% that neck formation was not progressed well. This result indicates that composites of 30 wt.% did not sinter enough.

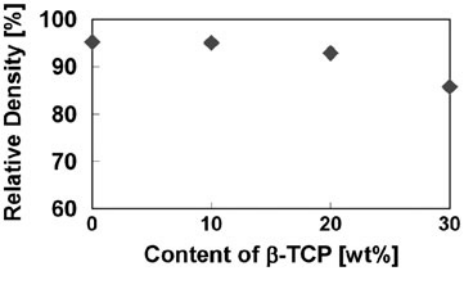

Figure 3. Relative density of HA/β-TCP composites.

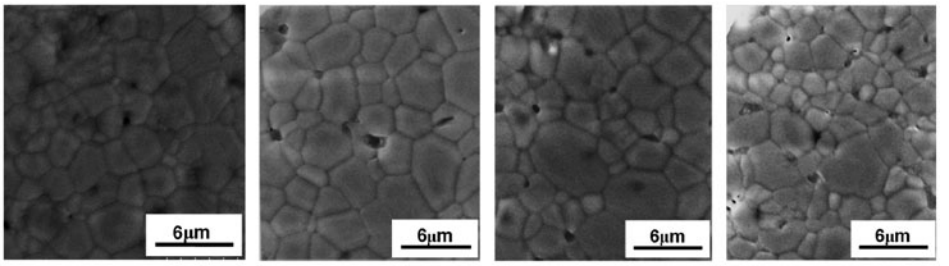

Figure 4. SEM photographs of grain size of HA/β-TCP.

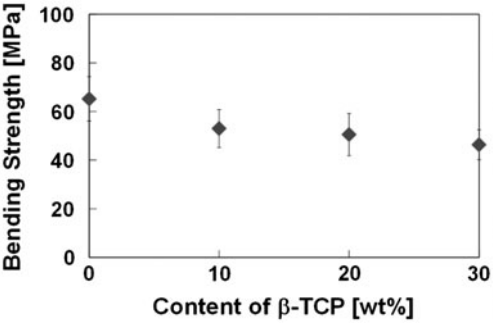

Figure 5. Bending strength of HA/β-TCP composites.

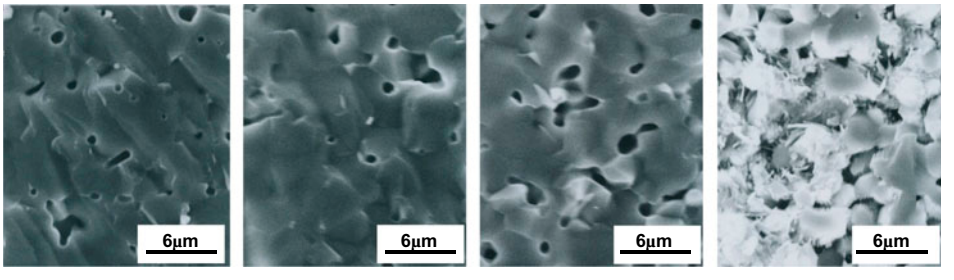

Figure 6. SEM photographs of fracture surface of HA/β-TCP.

Figures 7–9 show Vickers hardness, fracture toughness, and elastic coefficient of HA/β-TCP composites, respectively. It is found that Vickers hardness and elastic coefficient decreased with β-TCP content. In particular, those composite with 30 wt.% β-TCP decreased remarkably. This result is attributed to higher porosity in the composite. Fracture toughness slightly increased with β-TCP content. This is because of acting of pore in the composite as process zone in crack propagation.

Figure 10 shows XRD patterns of HA/β-TCP composites. The peaks of HA and β-TCP from software MDIJADE7 are plotted in the XRD patterns. It is found that XRD patterns of HA powder and HA/β-TCP (0 wt.%) have the same peaks. This indicates that the composition of HA did not change after sintering at 1250 °C. It is also

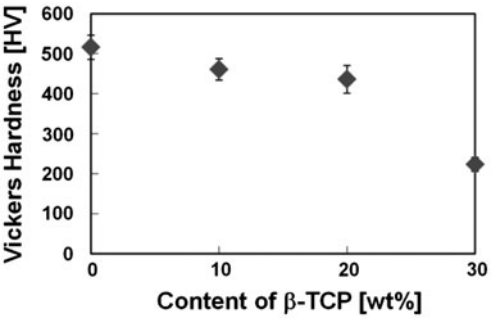

Figure 7. Vickers hardness of HA/β-TCP.

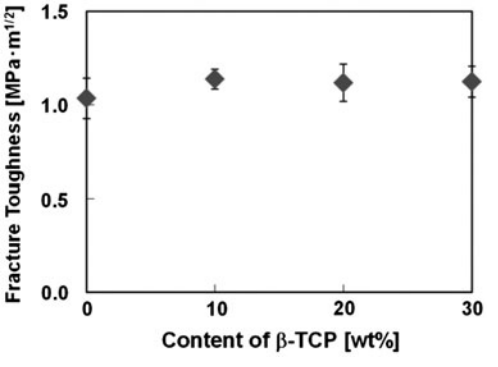

Figure 8. Fracture toughness of HA/β-TCP.

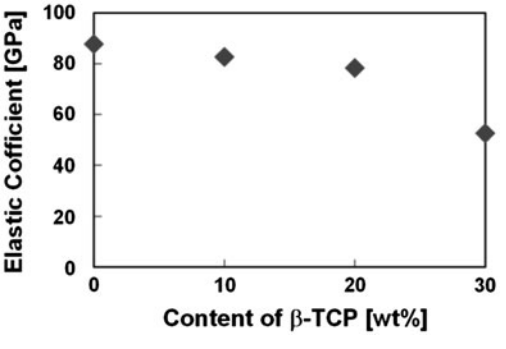

Figure 9. Elastic coefficient of HA/β-TCP.

found that composites include the peak of β-TCP around 31°. Generally, β-TCP transforms to α-TCP at 1120–1180 °C. However, the peak of α-TCP was not observed in Figure 10. It is suggested that β-TCP in HA/β-TCP composites was prohibited from transforming to α-TCP. Since α-TCP has lower density than β-TCP, volume expansion occurs when β-TCP transforms to α-TCP. Therefore, β-TCP in HA/β-TCP composites is affected by the mechanical restraint effect of HA, which caused the inhibition of volume expansion and resultant phase transformation of β-TCP.

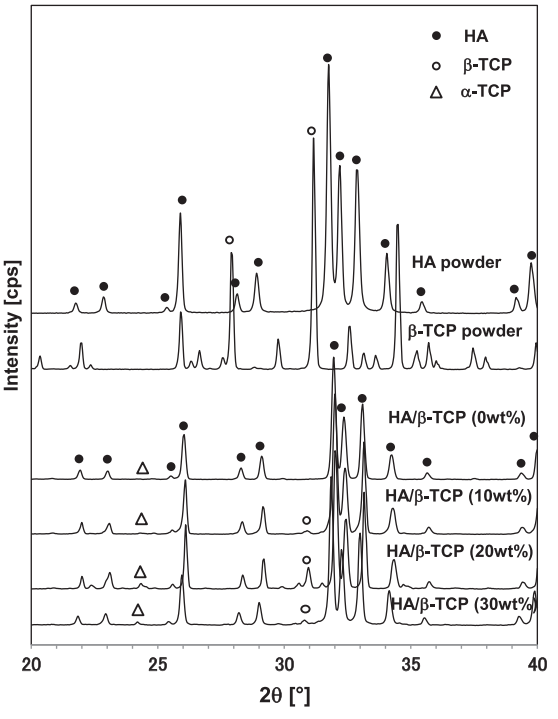

Figure 10. XRD pattern of HA/β-TCP composites.

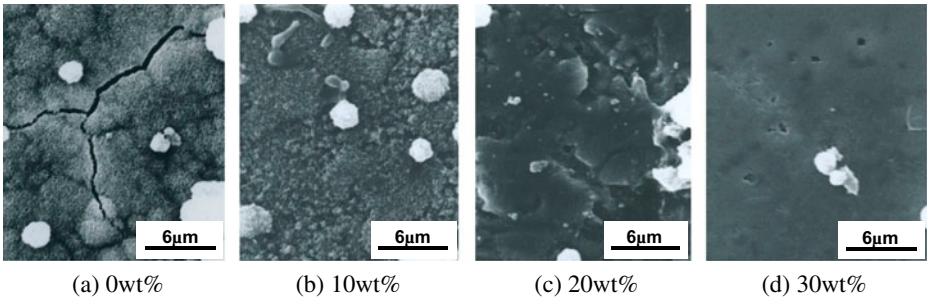

(a) 0wt% (b) 10wt% (c) 20wt% (d) 30wt%

Figure 11. SEM photographs of the surface of HA/β-TCP after one week soaking.

3.1.2. *Soaking test in SBF*

Figures 11 and 12 show SEM photographs of the surface of HA/β-TCP composites after one and three weeks soaking in SBF, respectively. It can be seen from Figure 11 that pure HA-formed apatite layer on its surface after one week soaking, which has similar morphology with Ref. [9], and a composite (10 wt.%) did not form apatite layer, but formed small crystals of apatite on its surface after one week soaking. Composites (20 and 30 wt.%) did not form apatite after one week soaking. It also can be seen from Figure 12 that all composites (0, 10, 20, and 30 wt.%) formed apatite on their surface after three weeks soaking. This result indicates that the rate of apatite formation for composites decreases comparing with pure HA and that the rate of apatite formation decreases with β-TCP content.

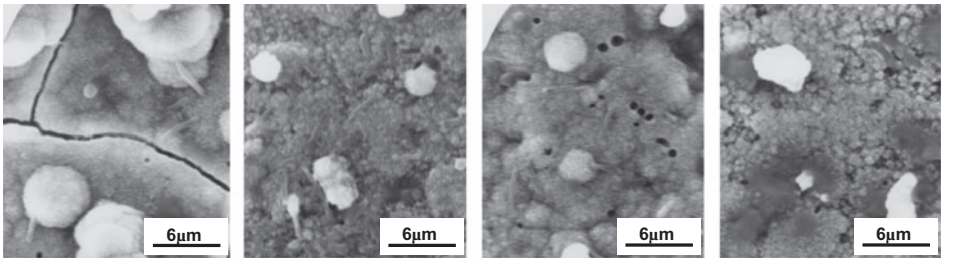

(a) 0wt% (b)10wt% (c) 20wt% (d) 30wt%

Figure 12. SEM photographs of the surface of HA/β-TCP after three weeks soaking.

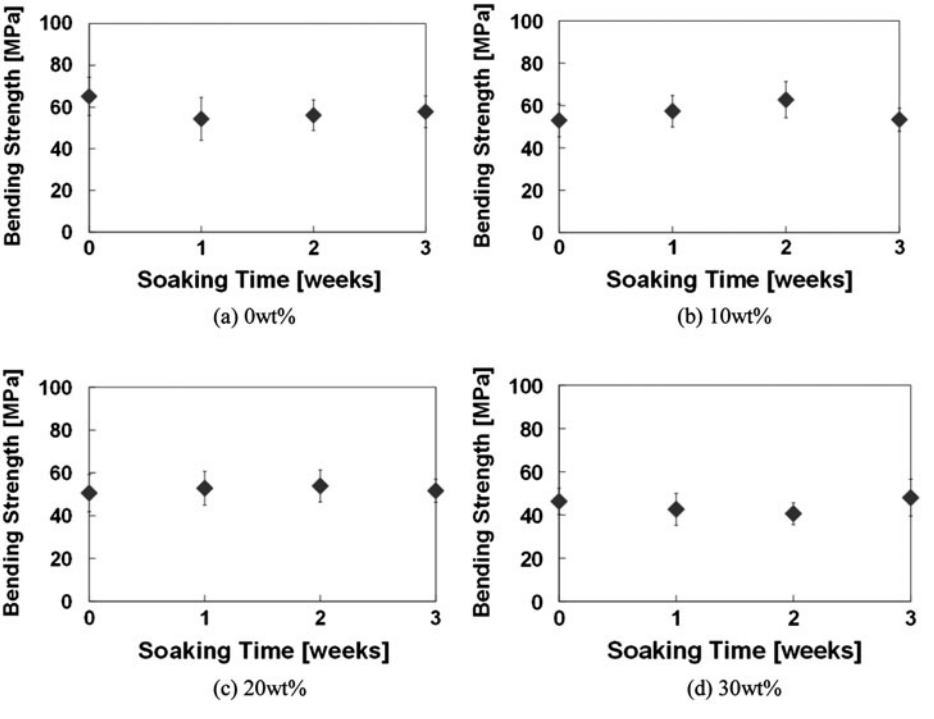

Figure 13. Bending strength of HA/β-TCP composites on each soaking condition.

Bending strength of HA/β-TCP composites was measured after soaking in SBF, as shown in Figure 13. The bending strength of pure HA (0 wt.%) decreased with soaking, however, the strength of composites (10, 20, 30 wt.%) did not decrease after soaking. This is because of the high dissolution reaction and successive apatite formation of pure HA (0 wt.%), and lower dissolution reaction of the surface of β-TCP,[10] respectively. Thus, it could be stated that the difference in surface reactivity affects the strength of composites in body environment significantly.

3.2. HA/β-TCP composites with sintering additive

3.2.1. Mechanical properties in atmosphere

As described above, the composites (30 wt.%) did not sinter enough. To improve the sinterability, composite (30 wt.%) was doped with 1 wt.% of silica (SiO_2) or magnesia

(MgO). Figure 14 shows relative density of HA/β-TCP/SiO_2 and MgO composites. It is found that shrinkage and relative density of HA/β-TCP/SiO_2 decreased compared with HA/β-TCP, whereas those of HA/β-TCP/MgO increased. This result indicates that SiO_2 did not act as a sintering additive, whereas MgO accelerates densification.

Figure 15 shows SEM photographs of the grain size of HA/β-TCP/SiO_2 or MgO composites. Figure 16 shows grain size of HA/β-TCP/SiO_2 or MgO composites calculated by Equation (4) using SEM photographs. It is found that grain size of HA/β-TCP/SiO_2 decreased in comparison to HA/β-TCP. From Figure 15(a), it is also apparent that neck formation did not progress in HA/β-TCP/SiO_2. This result means that HA/β-TCP/SiO_2 did not sinter enough. On the other hand, grain size of HA/β-TCP/MgO did not change in comparison to HA/β-TCP. As shown in Figure 15(b), it is

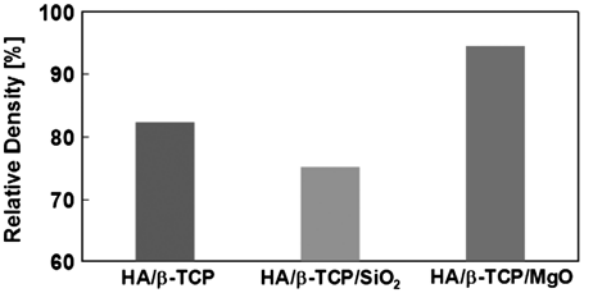

Figure 14. Relative density of HA/β-TCP/SiO_2 or MgO.

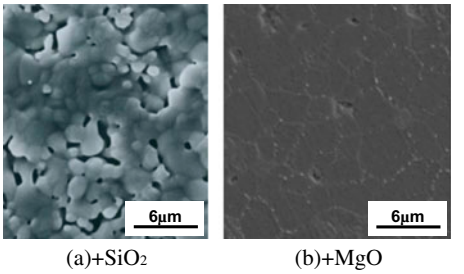

Figure 15. SEM photographs of the grain size of HA/β-TCP/SiO_2 or MgO.

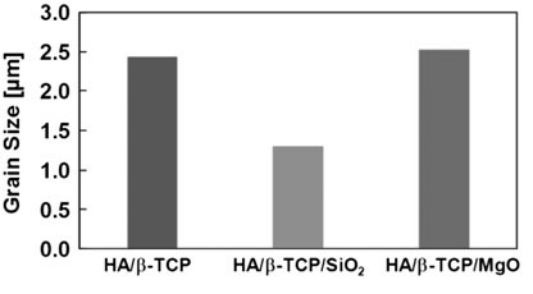

Figure 16. Grain size of HA/β-TCP/SiO_2 or MgO.

found that the abnormal grain growth of HA/β-TCP was inhibited by addition of MgO. Thus, it is speculated that addition of MgO had an effect on inhibiting of grain coarsening.

Figure 17 shows bending strength of HA/β-TCP/SiO_2 and MgO composites. It is found that bending strength of HA/β-TCP/SiO_2 composites slightly decreased by ~10% comparing to HA/β-TCP. On the other hand, HA/β-TCP/MgO increased by ~40% comparing to HA/β-TCP. Figure 18 shows SEM photographs of the fracture surface of HA/β-TCP/SiO_2 and MgO composites. In both samples, it is found that transgranular fracture occurred. The appearance of fracture surface of HA/β-TCP/SiO_2 was similar to that of HA/β-TCP. Therefore, it is confirmed that sinterability of HA/β-TCP/SiO_2 was not improved.

Figures 19–21 show Vickers hardness, fracture toughness, and elastic coefficient of HA/β-TCP/SiO_2 and MgO composites, respectively. For HA/β-TCP/SiO_2, cracks did

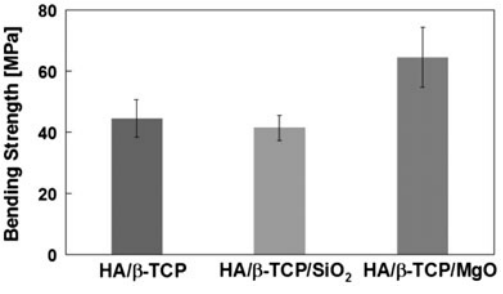

Figure 17. Bending strength of HA/β-TCP/SiO_2 or MgO.

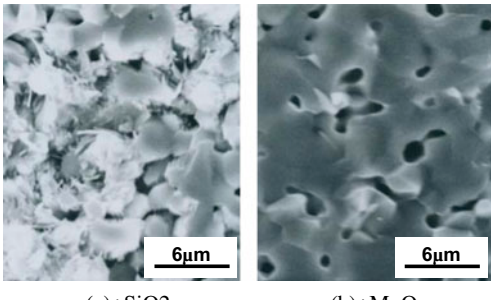

(a)+SiO2 (b)+MgO

Figure 18. SEM photographs of the fracture surface of HA/β-TCP/SiO_2 or MgO.

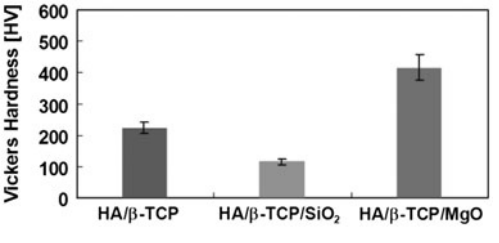

Figure 19. Vickers hardness of HA/β-TCP/SiO_2 or MgO.

not form on its surface, and the detachment was formed around indentation. Therefore, fracture toughness of HA/β-TCP/SiO_2 could not be measured. It is found that Vickers hardness and elastic coefficient decreased with SiO_2 addition, whereas they increased with MgO addition. Fracture toughness of HA/β-TCP/MgO is similar to HA/β-TCP.

Figure 22 shows XRD patterns of HA/β-TCP/SiO_2 or MgO composites, respectively. The peak of SiO_2 itself was observed in XRD pattern of HA/β-TCP/SiO_2. On the other hand, the peak of CaO was observed in XRD pattern of HA/β-TCP/MgO. These results also indicate that SiO_2 of HA/β-TCP/SiO_2 did not sinter enough as sintering additive.

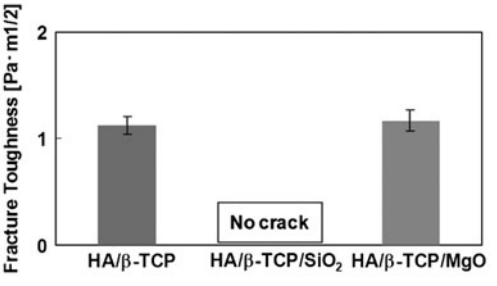

Figure 20. Fracture toughness of HA/β-TCP/SiO_2 or MgO.

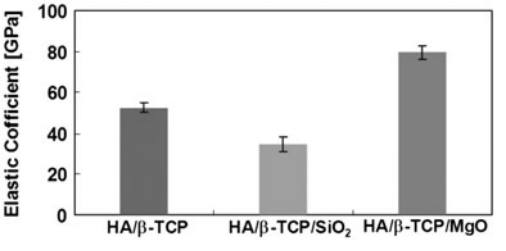

Figure 21. Elastic coefficient of HA/β-TCP/SiO_2 or MgO.

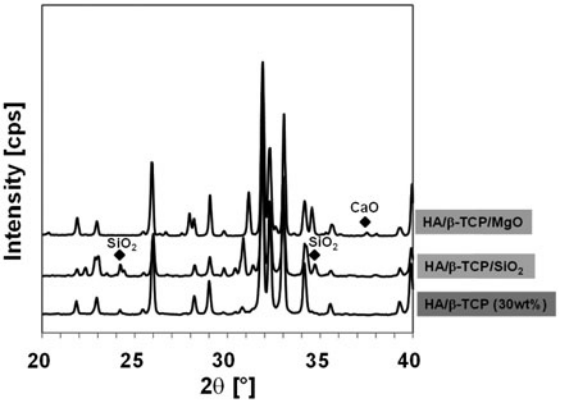

Figure 22. XRD pattern of HA/β-TCP/SiO_2 or MgO.

It is speculated that the difference in effectiveness as an additive is the different kind of chemical bonding of chemical compounds. The chemical bonding of SiO_2 is covalent binding, whereas that of MgO is ion binding. The covalent binding is comparatively strong, whereas the ion binding is comparatively weak. In case of ion binding, the binding is easily separated due to its weak chemical binding, therefore, atoms are easy to react into HA/β-TCP in sintering. These result led to high densification of HA/β-TCP/MgO. It was also reported that Mg of HA/β-TCP/MgO incorporates preferentially into β-TCP phase in HA/β-TCP, therefore, densification occurs during sintering.[6] As shown in Figure 22, the peak of CaO indicates the reaction that Mg atom of MgO displaced Ca atom of β-TCP occurred during sintering. It is also speculated that Mg easily displace Ca, because both Ca and Mg were atoms of second row of periodic table, and had similar characteristic.

3.2.2. Soaking test in SBF

Figure 23 shows SEM photographs of the surface of HA/β-TCP/SiO_2 or MgO composites after four weeks soaking in SBF. In comparison to HA/β-TCP (30 wt.%), it is found that the ability of apatite formation of HA/β-TCP/SiO_2 or MgO decreases.

Bending strength of HA/β-TCP/SiO_2 and MgO composites were measured after soaking in SBF, as shown in Figure 24. Bending strength of HA/β-TCP/SiO_2 decreased after soaking. This is because of the higher porosity due to the lower relative density of

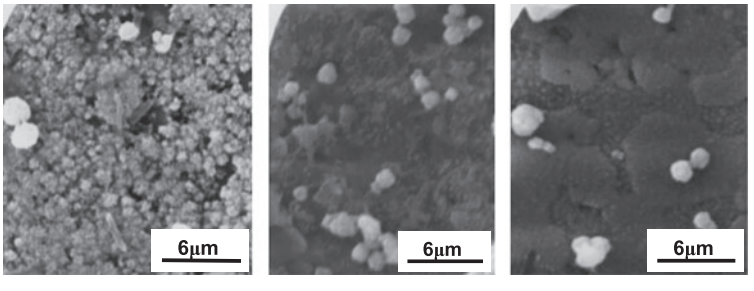

(a)HA/β-TCP (b)+SiO_2 (c)+MgO

Figure 23. SEM photographs of the surface of HA/β-TCP/SiO_2 or MgO after four weeks soaking.

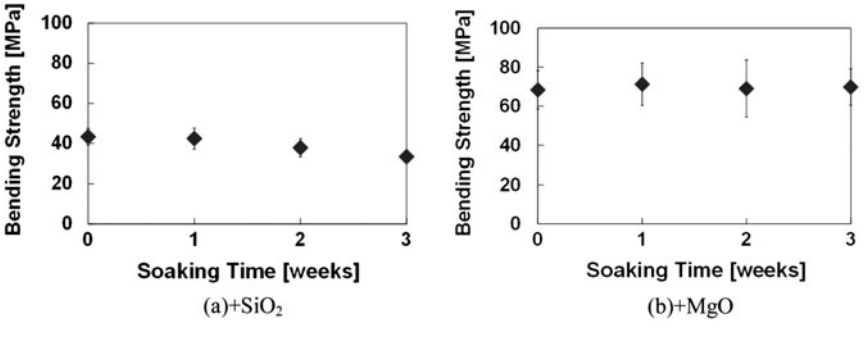

(a)+SiO_2 (b)+MgO

Figure 24. Bending strength of HA/β-TCP/SiO_2 or MgO on each soaking condition.

HA/β-TCP/SiO_2. As a result, SBF diffused into the composite and the dissolution occurred inside of the composite. On the other hand, bending strength of HA/β-TCP/MgO did not decrease after soaking, because of its low reactivity of the surface. It is indicated that the change in bending strength after soaking is related to its surface reaction in SBF and its porosity.

4. Conclusions

In this study, mechanical properties and bioactivity of HA/β-TCP composites which are prepared by sintering of HA and β-TCP powder mixture were investigated. The effect of addition of SiO_2 and MgO was also investigated. With increasing β-TCP content, relative density decreased and grain size increased. Bending strength of composites also decreased by ~20% due to β-TCP addition, because of lower relative density and larger grain size. Vickers hardness and elastic coefficient decreased with increasing β-TCP content. On the other hand, fracture toughness increased slightly due to β-TCP addition. The ability of apatite formation in SBF decreased with increasing β-TCP content. It is indicated that the change in bending strength after soaking related to its surface reaction in SBF and its porosity.

Because a composite (30 wt.%) had low sinterability, SiO_2 and MgO were added as sintering agents. As a result, it is found that MgO addition improved sinterability, however, SiO_2 did not. These results were attributed to high reactivity of MgO. It is found that the ability of apatite formation of HA/β-TCP/SiO_2 or MgO decrease.

References

[1] Akao M, Aoki H, Kato K. Mechanical properties of sintered hydroxyapatite for prosthetic applications. J. Mater. Sci. 1981;16:809–812.
[2] Akao M, Aoki H, Kato K, Sato A. Dense polycrystalline β-tricalcium phosphate for prosthetic applications. J. Mater. Sci. 1982;17:343–346.
[3] Metsger DS, Rieder MR, Foreman DW. Mechanical properties of sintered hydroxyapatite and tricalcium phosphate ceramic. J. Mater. Sci. Mater. Med. 1999;10:9–17.
[4] Raynaud S, Champion E, Lafon JP, Bernache-Assollant D. Calcium phosphate apatites with variable Ca/P atomic ratio. III. Mechanical properties and degradation in solution of hot-pressed ceramics. Biomaterials. 2002;23:1081–1089.
[5] Shiota T, Shibata M, Yasuda K, Matsuo Y. Influence of β-tricalcium phosphate dispersion on mechanical properties of hydroxyapatite ceramics. J. Ceram. Soc. Jpn. 2008;116:1002–1005.
[6] Ryu H-S, Hong KS, Lee J-K, Kim D, Lee JH, Chang B-S, Lee D-H, Lee C-K, Chung S-S. Magnesia-doped HA/β-TCP ceramics and evaluation of their biocompatibility. Biomaterials. 2004;25:393–401.
[7] Hench LL. The story of bioglass®. J. Mater. Sci. Mater. Med. 2006;17:967–978.
[8] Kokubo T. Bioactive glass ceramics: properties and applications. Biomaterials. 1991;12:155–163.
[9] Kobayashi S, Kawai W. Development of carbon nanofiber-reinforced hydroxyapatite with enhanced mechanical properties. Composites Part A. 2007;38:114–123.
[10] Uchino T, Ostuki C, Kamitakahara M, Miyazaki T. Apatite formation behavior on tricalcium phosphate (TCP) porous body in a simulated body fluid. Key Eng. Mater. 2006;251:309–311.